




Article

Flexible Hydrogen Peroxide Sensors Based on Platinum Modified Free-Standing Reduced Graphene Oxide Paper

Run-Min Song ¹, Zhan-Hong Li ¹ , Peng-Ju Wei ¹, Xue-Ling Zhao ¹, Cheng Chen ¹ 
and Zhi-Gang Zhu ^{1,2,*} 

¹ School of Environmental and Materials Engineering, College of Engineering, Shanghai Polytechnic University, 2360 Jinhai Road, Shanghai 201209, China; runminsong@163.com (R.-M.S.); zhli@sspu.edu.cn (Z.-H.L.); pjweisspu@163.com (P.-J.W.); xlzhao@sspu.edu.cn (X.-L.Z.); chencheng@sspu.edu.cn (C.C.)

² Shanghai Innovation Institute for Materials, Shanghai 200444, China

* Correspondence: zgzhuzhu@sspu.edu.cn; Tel.: +86-21-50215021 (ext. 8325)

Received: 9 April 2018; Accepted: 14 May 2018; Published: 23 May 2018



Abstract: In this article, we report a facile method to fabricate free-standing reduced graphene oxide paper (rGOP) by vacuum filtration. Pt nanoparticles were electrodeposited on reduced graphene oxide paper to construct a sensitive and flexible hydrogen peroxide (H₂O₂) sensor. The properties of Pt/rGOP were characterized by scanning electron microscopy, energy dispersive X-ray, X-ray photoelectron spectroscopy and Raman spectroscopy. The electrochemical characterizations of the resulting sensor were carried out by cyclic voltammetry, chronoamperometry and electrochemical impedance spectroscopy. The Pt/rGOP hybrid electrode had an excellent electrochemical property, with superb electrocatalytic activity, a large electrochemical active surface area, flexibility and high stability. The linear ranges of the as-prepared sensor for H₂O₂ detection were divided into two linear sections: 0.2 μmol/L to 2.0 mmol/L and 2.0 to 8.5 mmol/L, with a detection limit of 100 nmol/L (S/N = 3) and a response time of less than 5 s. The proposed sensor has great potential to become a reliable and flexible tool in biosensor and point-of-care medical devices.

Keywords: reduced graphene oxide paper; hydrogen peroxide; electrodeposition; Pt nanoparticles; biosensor

1. Introduction

Hydrogen peroxide (H₂O₂) is one of the products during enzyme catalyzing, such as glucose oxidase, which is closely related to diverse physiological and pathological consequences including aging, organ injury and cancer, has received enormous attentions in academy and industry [1–6]. There is great need to detect H₂O₂ in environmental, industrial and clinic fields [7]. Thus, it is critical to develop a novel method for the accurate and quick detection of H₂O₂. During the past few decades, many techniques have been established to detect H₂O₂, such as fluorimetry [8], titrimetry [9], chemiluminescence [10], spectrophotometry [11], chromatography [12], colorimetry [13], electron spin resonance spectroscopy [14], electrochemical methods [15,16], and so on. Among these techniques, electrochemical methods have attracted wide attention for real-time detection of H₂O₂ because of their high sensitivity, fast response and low cost. At present, the electrochemical sensors used for detection of H₂O₂ are mainly classified into enzymatic and nonenzymatic sensors. Compared to enzymatic sensors, the nonenzymatic sensors composed of transition metal nanoparticles (NPs), such as Pt, Ag, Au, Ni, etc., have generated a great deal of interest, thanks to their outstanding long-term stability/sensitivity regardless of the intrinsic nature of enzymes [17–20].

Carbon-based materials, such as graphene and carbon nanotubes, have become a hot spot in many research fields [20,21]. Graphene is a two-dimensional material with a layer of sp^2 C atoms tightly packed into a honeycomb lattice. It possesses extraordinary mechanical, thermal and electronic properties [22,23]. Moreover, the large surface area and good electronic properties of graphene are considered advantages of an alternative electrode material for sensors [24,25]. Until now, several methods have been used to synthesize graphene, such as chemical vapor deposition [26], electrochemical exfoliation [27], micromechanical exfoliation [22], thermal growth from silicon carbide [28], etc. Among these methods, a solution-based method is thought to be the most promising route to produce large quantities of graphene [29]. Graphene oxide (GO) can be reduced by different methods, including chemical [30–32], thermal [33], electrochemical [34–36] and microwave-assisted techniques [37,38]. So far, GO can be manufactured into free-standing reduced graphene oxide paper (rGOP), with thicknesses ranging from 1 to 30 μm [39]. Such rGOPs have preferable extension and tensile properties (32 GPa) compared to graphite foils, bulky papers and other paper-like materials [39]. The combination of the superior mechanical strength, high electrical conductivity (7200 S m^{-1}), thermal stability, structural uniformity and biocompatibility enables rGOP to be an ideal material for many technological applications [40,41].

In this article, we report a nonenzymatic biosensor based on free-standing reduced graphene oxide paper modified with Pt nanoparticles (PtNPs). Free-standing reduced graphene oxide paper could be an alternative to the traditional glassy carbon electrode, as the substrate for detection of H_2O_2 . The schematic illustration of the fabrication process for a Pt/rGOP electrode is shown in Figure 1. Test results reveal that electrodeposition of PtNPs on free-standing reduced graphene oxide paper has two good linear responses to H_2O_2 , ranging from 0.2 $\mu\text{mol/L}$ to 8.5 mmol/L , with a detection limit of 100 nmol/L ($\text{S/N} = 3$). The as-prepared flexible and free-standing reduced graphene oxide paper has great potential in real applications, especially for biosensor and point-of-care medical devices.

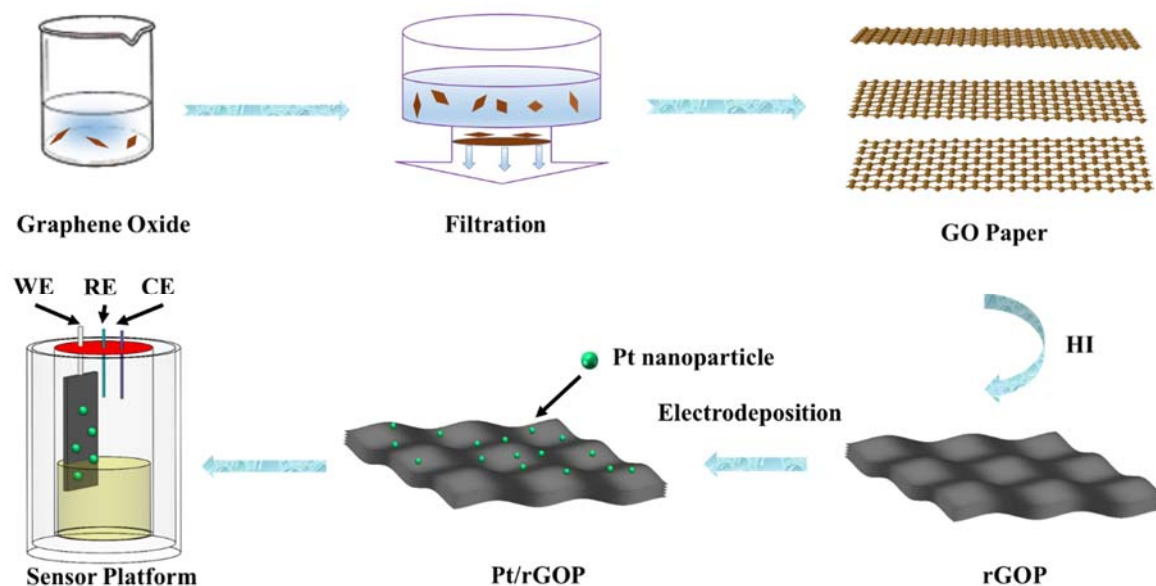


Figure 1. Illustrative fabrication process of the Pt/rGOP electrode for detection of hydrogen peroxide.

2. Experimental Section

2.1. Materials

Graphene oxide (10 mg/mL) aqueous solution was purchased from ACS Materials (Shanghai, China). Filter paper (mixed cellulose membrane) with a diameter of 50 cm and a pore size 0.22 μm was purchased from Xin Ya Purification Equipment Co. Ltd. (Shanghai, China). Hydrogen

hexachloroplatinate (IV) hydrate ($\text{H}_2\text{PtCl}_6 \cdot 6\text{H}_2\text{O}$), hydrogen peroxide (H_2O_2) and hydroiodic acid (HI, 45% in water) were purchased from Sinopharm Chemical Reagent Co. Ltd. (Shanghai, China). Ascorbic acid (AA), glucose (Glu), fructose (Fru), uric acid (UA), oxalic acid (OA) and citric acid were obtained from Sigma-Aldrich (Shanghai, China). All other chemicals used were of analytical grade, without need of further purification. Phosphate buffer solution (PBS) was made of potassium dihydrogen phosphate (KH_2PO_4) and disodium hydrogen phosphate (Na_2HPO_4) at pH = 7.4.

2.2. Preparation of Pt NPs Modified rGOP

Graphene oxide aqueous solution (GO 10 mg/mL) was diluted with deionized (DI) water to 2 mg/mL; the free-standing graphene oxide paper (GOP) was fabricated, using a vacuum filtration method, by filtrating 20 mL of 2 mg/mL GO. The beauty of this facile method is that the thickness of the graphene oxide paper could be easily controlled by adding different volumes of GO solution. When most of the water had been filtered by a vacuum filtration machine, a round and integral layer of graphene oxide paper with a smooth surface could be obtained. The graphene oxide adhered-to filter paper was then put in the oven at 60 °C for 5 min to evaporate the remaining water. The as-prepared GOP was easily peeled off from the filter paper without any cracks. Then, GOP was chemically reduced by being immersed in 45% HI solution in a sealed cuvette at room temperature for 1 h. The HI-reduced graphene oxide paper was rinsed with DI water and ethanol several times, and the reduced graphene oxide paper was dried at room temperature.

A conventional three-electrode system was employed for electrodeposition, while platinum net and saturated calomel electrode (SCE) were used as counter and reference electrodes, respectively. Before electrodeposition, rGOP was tailored to several sheets at 7 mm × 20 mm. Electrochemical deposition of PtNPs on rGOP was performed in 0.5 mol/L H_2SO_4 solution in the presence of 1 mmol/L H_2PtCl_6 , added using cyclic voltammetry. The potential ranged from −0.2 V to 1.25 V with a scan rate of 50 mV/s, and the effect of different cycles (5, 10, 15, 20 and 25 cycles) was evaluated. After electrodeposition, the rGOP modified with PtNPs was rinsed thoroughly with DI water several times to remove residual electrolytes and then dried at room temperature.

2.3. Characterization and Electrochemical Measurements

The morphology of the rGOP was investigated by field emission scanning electron microscopy (FE-SEM, S-4800, Hitachi Co. Ltd., Tokyo, Japan) at an accelerating voltage of 10 kV. The distribution of elements in crystals was characterized using an energy dispersive X-ray spectrometer (EDX) that was attached to SEM. Raman spectrum (SENTERRA, Karlsruhe, Germany) was used for showing the intrinsic structure between GOP and rGOP. The compositional analysis of the samples was checked by X-ray photoelectron spectroscopy (XPS, ESCALAB250Xi, Thermo Scientific, Waltham, USA). Chronoamperometry, cyclic voltammetry (CV) and electrochemical impedance spectroscopy (EIS) were carried out using an electrochemical workstation (CHI-760E CH Instruments, Shanghai, China). Both CV and EIS measurements for rGOP were performed in PBS (pH 7.4). Chronoamperometry was used to investigate the sensing performance of electrodes. Different potentials of 0, −0.05, −0.1, −0.15, −0.2, −0.25 and −0.3 V were set to carry out the optimization. Before measurement, all solutions used in electrochemical tests were bubbled with high pure nitrogen for 15 min to thoroughly remove oxygen from the solution.

3. Results and Discussion

3.1. Characterization of rGOP

Free-standing rGOP is fabricated through vacuum filtration, followed by chemical reduction in HI aqueous solution. It is a facile process to control the thickness of free-standing rGOP by adding different volumes of GO aqueous suspension, as shown in Figure 2. Chemical reduction by HI could effectively remove most oxygen-functional groups and the covalent bond structure in GOP. Compared

to GOP, rGOP has an improved electron transfer ability, is silvery in color and shows metallic gloss on both sides. The as-prepared rGOP is highly flexible and can be randomly folded; one of them was formed into a paper crane (Figure 2A). The morphology of rGOP is characterized by SEM with high magnification, as shown in Figure 2B,C. The images reveal that rGOP is constructed layer-by-layer by parallel rGOP nanosheets, with uniform thickness throughout its cross-section. The rGOP is intensely crumpled, and the typical wrinkled nanostructure is caused by the overlap of graphene nanosheets after chemical reduction (Figure 2D).

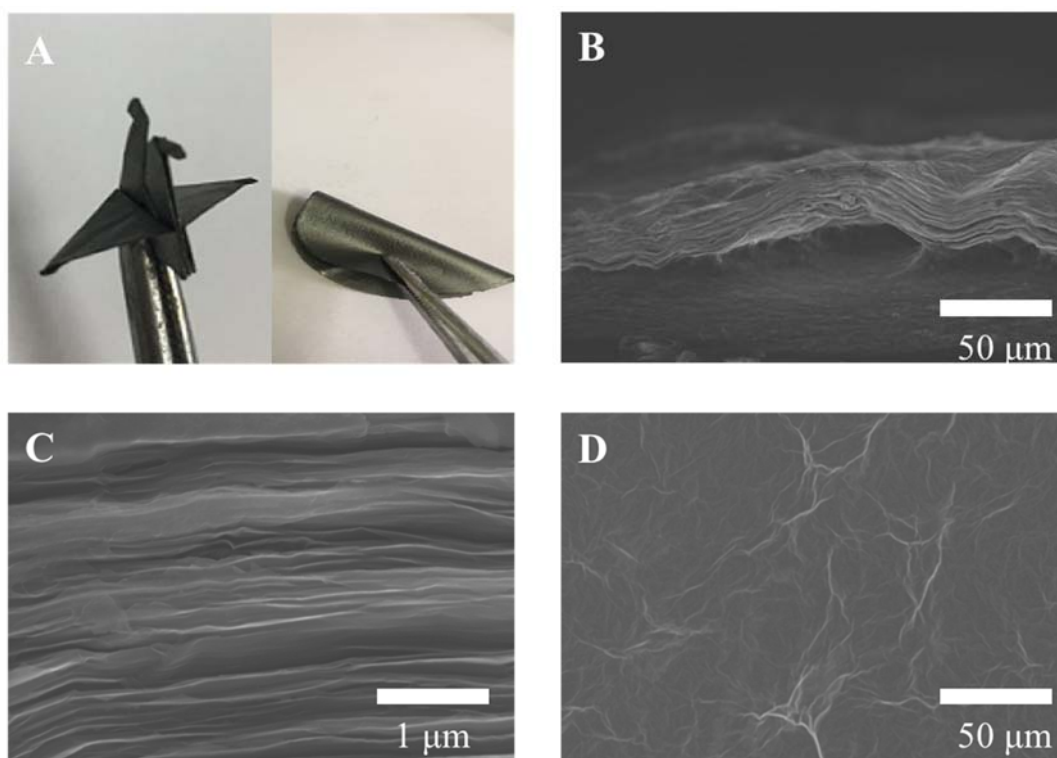


Figure 2. (A) Digital photo of rGOP. SEM images of rGOP, with (B) and (C) cross-section view and (D) top view.

To examine the surface chemical composition and electronic states of the elements, X-ray photoelectron spectroscopy (XPS) was used. The results are presented in Figure 3 for GOP and rGOP, with or without PtNPs. Figure 3A shows that there are big differences in C 1s peaks between GOP and rGOP in XPS spectra. The two peaks with a binding energy of 284.6 eV (C=C/C-C) and 286.8 eV (C-O) are clearly exhibited in the GOP spectrum. After reduction, the main peak in rGOP greatly decreases to around 284.8 eV, which is attributed to C-O. This clearly demonstrates that GOP was successfully reduced to rGOP by HI reduction method. As Figure 3B shows, the peaks with a binding energy of 74.58 eV and 71.18 eV are related to Pt 4f_{5/2} and Pt 4f_{7/2}, respectively, indicating that the Pt is mainly metallic in Pt/rGOP [42].

Raman spectroscopy is an important experimental method in graphene research, which provides information about the structural defects and graphite structure of GOP and rGOP. As illustrated in Figure 4, the Raman spectra of GOP and rGOP have two obvious peaks. The peak at 1344 cm⁻¹ is named the D band, which is related to the degree of defect in the lattice of graphene structure. The peak at 1586 cm⁻¹ is named G band, which is assigned to the first-order scattering of the E_{2g} mode of GO and corresponds to the in-plane vibration of sp²-bonded carbon atoms in a 2D hexagonal lattice [43]. The intensity ratio of G band over D band, I_G/I_D ratio, is widely used to estimate the density of defects in graphene structures: the smaller the value of I_G/I_D ratio, the higher the defect density [44].

The value of I_G/I_D decreased from 0.916 to 0.696 once the GOP reduced to rGOP. The decrement of I_G/I_D indicates that rGOP has more sp^3 electronic configurations and defects in the carbon atoms lattice structure when GOP is reduced to rGOP. After electrodeposition of PtNPs, the value of I_G/I_D increased from 0.696 to 0.812, which suggests that PtNPs, electrodeposited between rGOP layers, may reduce the defect density.

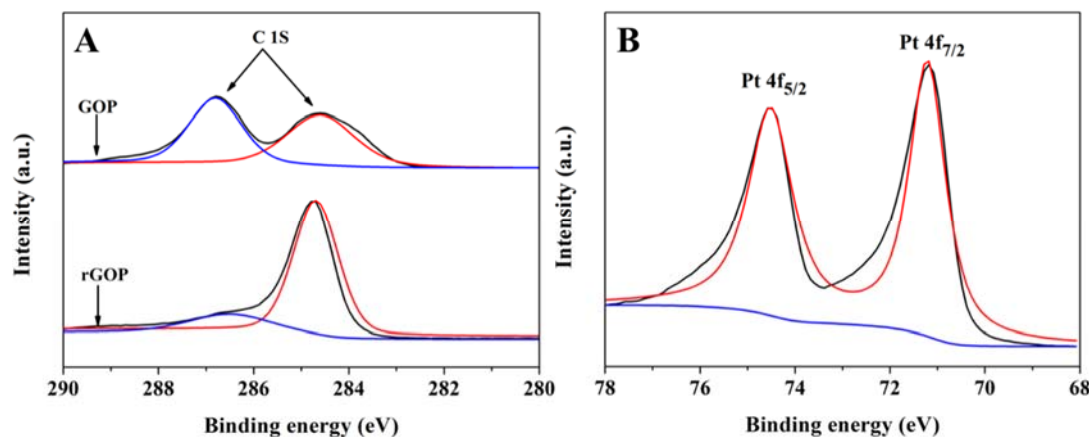


Figure 3. XPS spectra of (A) C 1s peak for GOP and rGOP (red line and blue line are the fitting curves). (B) Pt 4f peak for rGOP.

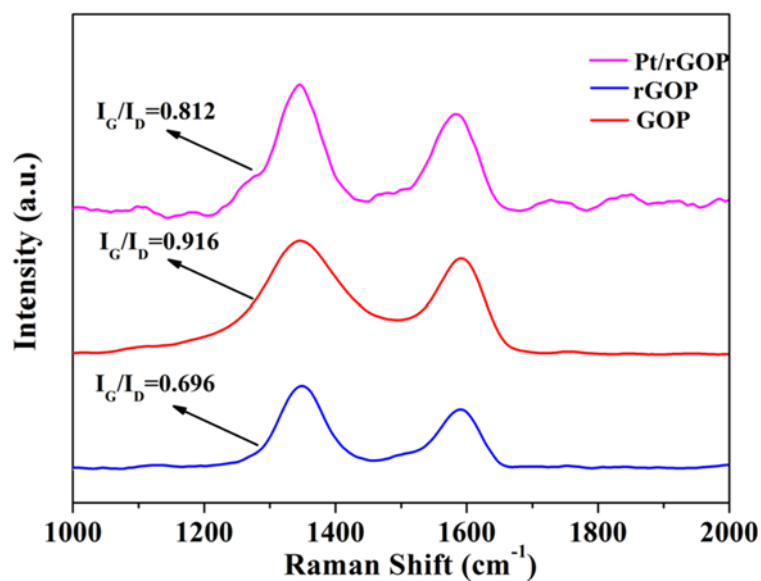


Figure 4. Raman spectra of GOP, rGOP and Pt/rGOP.

Pt nanoparticles were electrodeposited by cyclic voltammetry with different cycles (5, 10, 15, 20, 25 cycles) in a solution of 1 mmol/L H_2PtCl_6 and 0.5 mol/L H_2SO_4 . The same magnification was selected to determine the morphologies and distribution of Pt nanoparticles on rGOP, as the FESEM images show in Figure 5A–E. Figure 5A shows that Pt nanoparticles were electrodeposited by 5 cycles on rGOP. SEM images (Figure 5B–D) of Pt nanoparticles, obtained by different electrodeposition cycles, indicate that the diameter of Pt nanoparticles is less than 30 nm, and that they are homogeneously distributed on the rGOP without obvious agglomeration. Figure 5E shows that the obvious agglomeration occurred when the electrodeposition cycles were up to 25. The EDX spectrum of rGOP-PtNPs is shown in Figure 5F, which depicts the existence of C, O and Pt. C and Pt can easily

be attributed to the rGOP and PtNPs. The existence of O may be attributed to the adsorbed oxygen species of rGOP when using CV method to electrodeposit PtNPs.

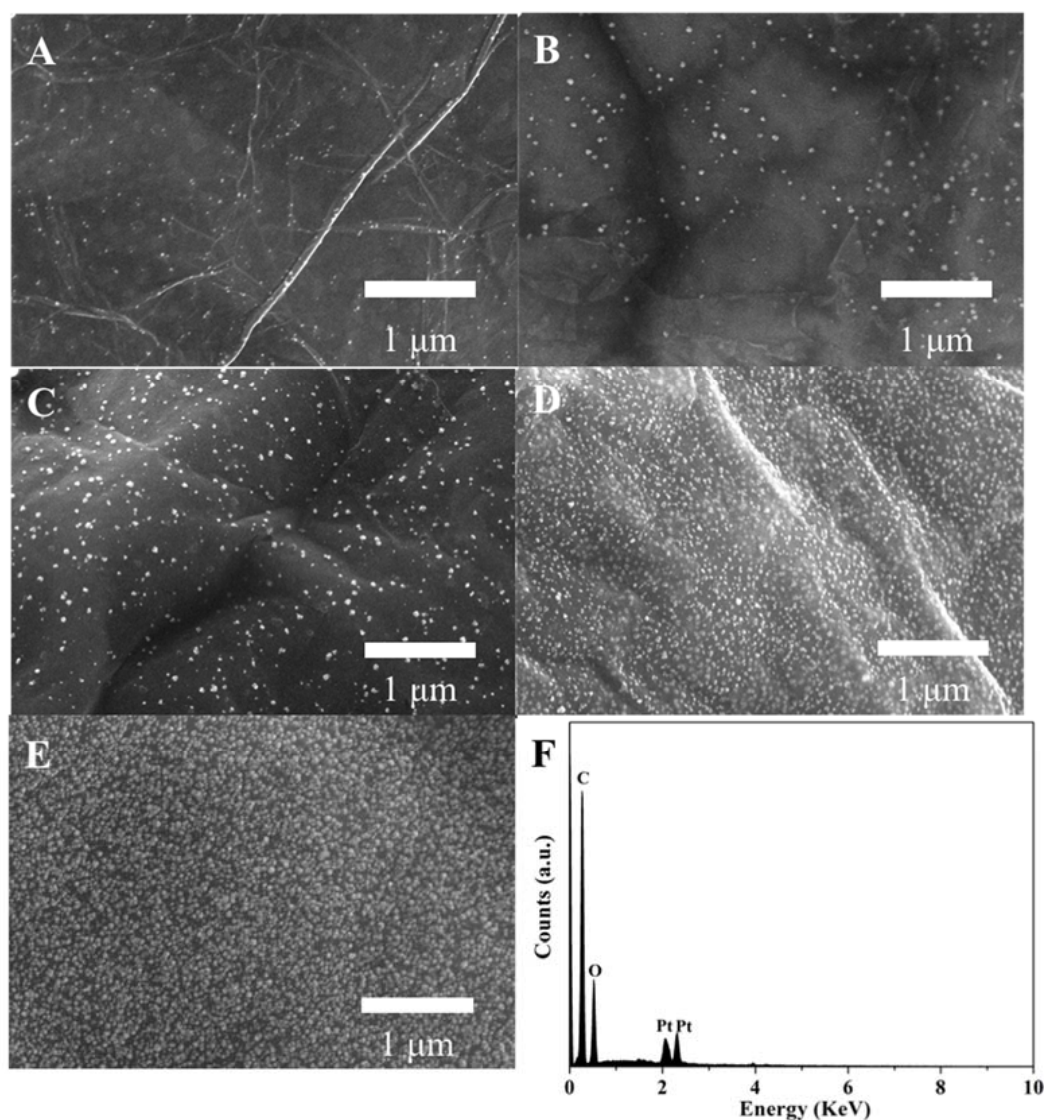


Figure 5. FESEM images of PtNPs on rGOP (A–E), with different deposition cycles and its (F) EDX analysis.

3.2. Electrochemical Characterization

CV curves of the Pt/rGOP electrode, scanned in deaerated 0.5 mol/L H_2SO_4 solution within a potential range from -0.2 V to 1.25 V, is shown in Figure 6A. The peak at 0.3 V is associated with the reduction of Pt oxide species. In Figure 6A, the peak of Pt species is invisible, but the analysis of previous data showed that PtNPs were successfully electrodeposited. Additionally, it is obvious that, once PtNPs were electrodeposited on the free-standing graphene paper, the current of Pt/rGOP charge and discharge became much larger than rGOP and Pt foil, indicating Pt/rGOP has the highest surface area. The electrochemical sensing performances of Pt foil and Pt/rGOP have been investigated in 0.1 mol/L PBS (pH = 7.4) containing 1.0 mmol/L H_2O_2 at a scan rate of 50 mV/s, as depicted in Figure 6B. Compared to the Pt foil, Pt/rGOP has a higher reduction current in the presence of H_2O_2 , reflecting that Pt/rGOP has superior electrochemical activity. EIS is often used to gain important information about the interfacial properties of electrodes, and Figure 6C exhibits the Nyquist plots

of Pt/rGOP and rGOP in the presence of 0.1 mol/L KCl containing 1 mmol/L $[\text{Fe}(\text{CN})_6]^{-3/-4}$. It is obvious that the charge-transfer resistance of the Pt/rGOP is much smaller than rGOP. This is mainly attributed to the high loading of PtNPs, with their uniform distribution and construction of an effective conduction pathway to boost the electron transfer on rGOP.

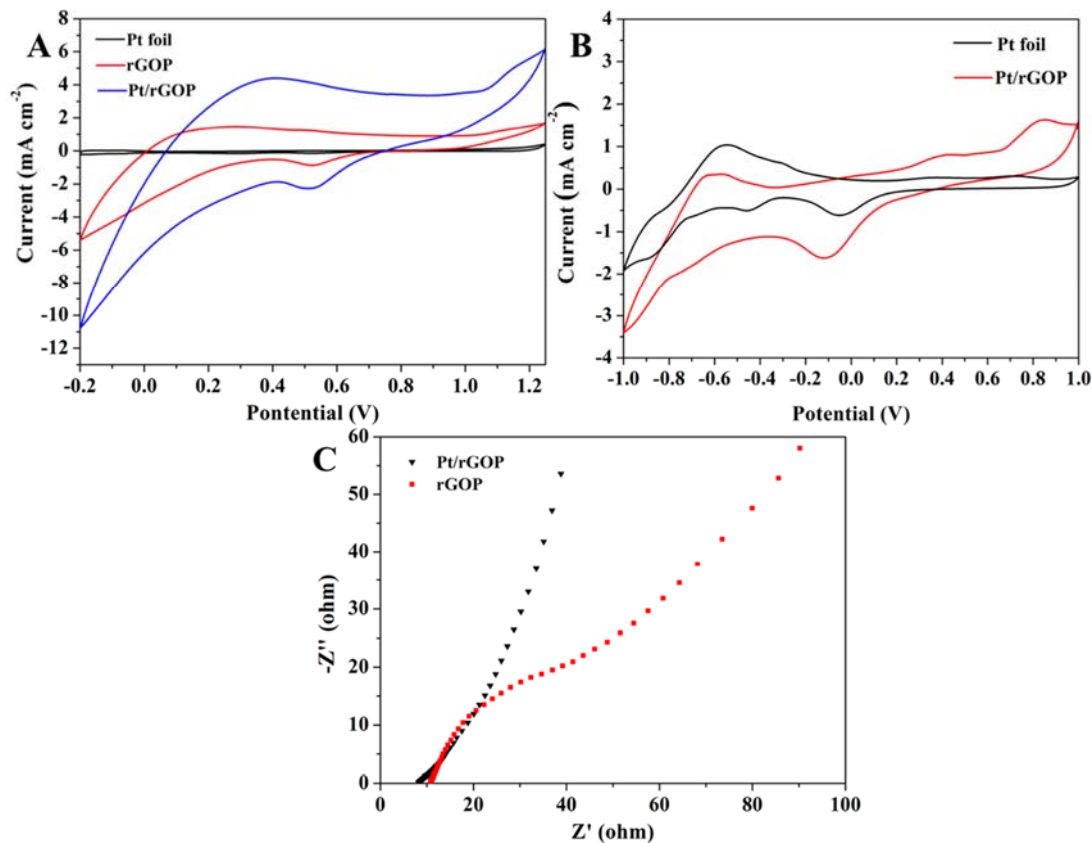


Figure 6. CV curves of (A) Pt foil, rGOP and Pt/rGOP in deaerated 0.5 mol/L H₂SO₄ with a scan rate of 50 mV/s, and (B) Pt foil and Pt/rGOP in 0.1 mol/L PBS containing 1.0 mmol/L H₂O₂ saturated with nitrogen gas. (C) Nyquist plots of Pt/rGOP, rGOP electrodes in deaerated 0.1 mol/L KCl, containing 1.0 mmol/L K₃Fe(CN)₆ and 1.0 mmol/L K₄Fe(CN)₆. Frequency range: 0.1–10⁵ Hz.

3.3. Amperometric Response to Hydrogen Peroxide

Figure 7A shows the amperometric responses of Pt/rGOP towards H₂O₂ at different applied potentials (0.0 to −0.3 V). The result reveals that Pt/rGOP exhibits the highest current density once the applied potential was −0.25 V. Figure 7B depicts the amperometric response changes with the different electrodeposition cycles. The current density gradually increased, with the electrodeposition cycles increased from 5 to 20, and further to 25, and the current density substantially reduced. This is because PtNPs exhibit an agglomerating phenomenon, comparing with the specimen deposited for 20 cycles. The result demonstrates that electrodeposition for 20 cycles in rGOP could obtain the largest electroactive area.

The amperometric response of Pt/rGOP to successive additions of different concentrations of H₂O₂ in 0.1 mol/L PBS with potential applied at −0.25 V is given in Figure 7C. It shows the sensor has a fast response and the current is able to reach a dynamic equilibrium within 5 s after adding H₂O₂. The fast response indicates a favorable electron transfer between Pt/rGOP and H₂O₂. It is found that the amperometric responses towards H₂O₂ concentration is wide, from 0.2 μmol/L to 8.5 mmol/L, and the detection ranges are divided into two linear sections: 0.2 μmol/L to 2.0 mmol/L and 2.0 to 8.5 mmol/L, while the sensitivities are 67.51 μA cm⁻² mM⁻¹ and 40.21 μA cm⁻² mM⁻¹, respectively,

as shown in Figure 7D. The existence of two linear ranges could indicate different mechanisms: at low concentrations of hydrogen peroxide, the electrocatalytic mechanism is dominant. Otherwise, at high concentration of hydrogen peroxide, the direct reduction of hydrogen peroxide on the surface can play an important role in the analytical signal [45]. Moreover, the detection limit of H_2O_2 can be as low as 100 nmol/L, at a signal-to-noise (S/N) ratio of 3. The sensor provides a more comparable detection limit and linear range compared to previous reports, as listed in Table 1. In the meantime, Pt/rGOP exhibits the highest sensitivity among all the sensors.

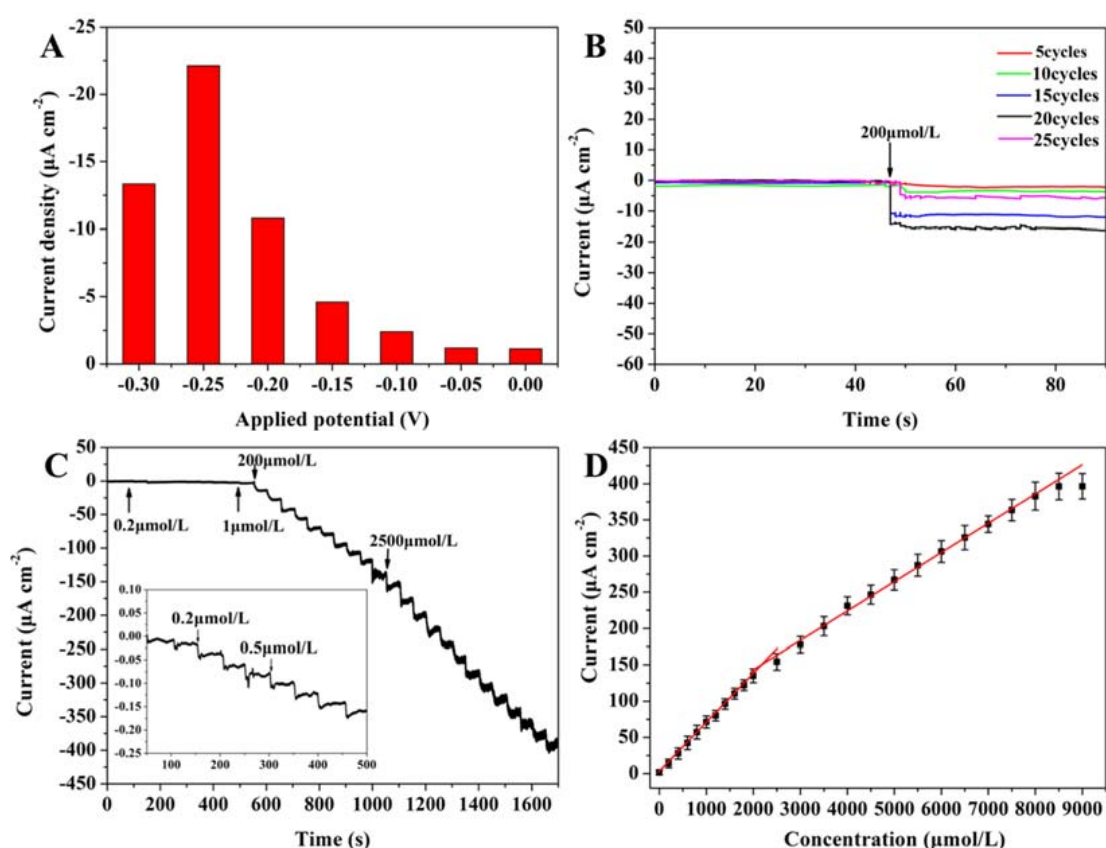


Figure 7. (A) Histograms of the current responses of Pt/rGOP electrode to 0.2 mmol/L H_2O_2 in PBS at a different applied potential. (B) Amperometric responses of the different deposition cycles on Pt/rGOP electrode to 0.2 mmol/L H_2O_2 in PBS at -0.25 V. (C) Typical amperometric response of Pt/rGOP electrode to successive additions of different hydrogen peroxide concentrations in PBS (pH 7.4) with magnetic stirring and its (D) calibration curve.

Table 1. Comparison of various graphene-based electrodes for H_2O_2 sensing.

Electrode	Sensitivity ($\mu\text{A cm}^{-2} \text{ mmol}^{-1}$)	LOD ($\mu\text{mol/L}$)	Linear Range ($\mu\text{mol/L}$)	Ref.
Au@PB NPs graphene paper	5.0	0.1	1–30	[46]
AuNPs/graphene paper	0.24	2	5–8600	[47]
PtNPs/graphene film	0.56	0.2	0–2500	[48]
PtNPs/MnO ₂ nanowires/graphene paper	0.13	1	2.0–13.3	[49]
HRP/graphene paper	0.56	1.7	3.5–329	[50]
AgNCs/graphene film	0.18	3.0	20–10,000	[51]
AuNPs-Porous graphene film	0.08	0.1	0.5–4900	[52]
PtNPs/graphene paper	67.51	0.1	0.2–2000	This work
PtNPs/graphene paper	40.21		2000–8500	This work

3.4. Stability and Bending Tests

The reproducibility and long-term stability of the Pt/rGOP were determined by evaluating the amperometric current response towards 0.2 mmol/L H_2O_2 in 0.1 mol/L PBS. The amperometric current responses of 5 sensors, fabricated under the same conditions, were tested for 10 days. This revealed that Pt/rGOP electrodes exhibit a relative standard deviation (RSD) of 3.8% for 10 days, signifying that the Pt/rGOP possesses high reproducibility and stability (Figure 8A). The flexibility is an important factor for flexible Pt/rGOP electrodes, and five Pt/rGOP electrodes were bent 180° up to 200 times, as shown in Figure 8B. The results show that it retains nearly 92% of original response after being bent 200 times. This proves that the flexible Pt/rGOP electrodes have excellent mechanical stability for electrochemical devices to detect H_2O_2 .

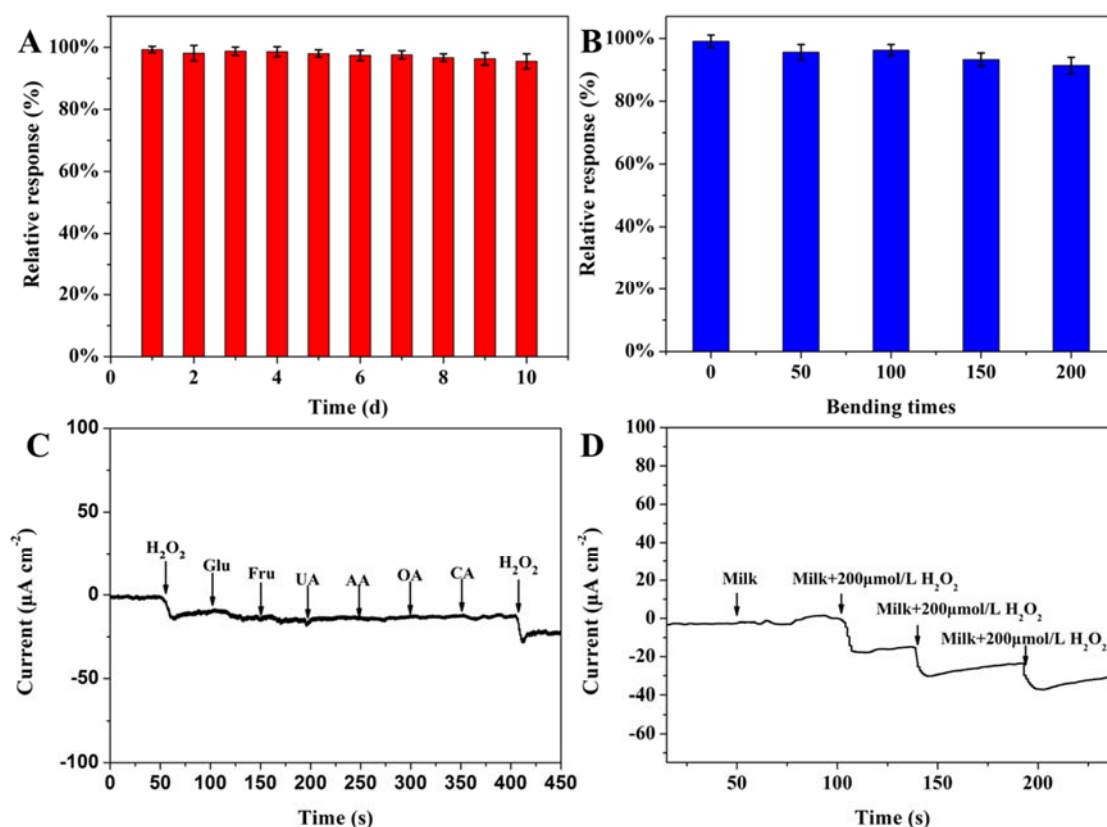


Figure 8. (A) Long-term stability test of the Pt/rGOP. (B) Effects of bending times on the current response to 10 $\mu\text{mol/L}$ of H_2O_2 of the flexible Pt/rGOP electrode. (C) Amperometric responses upon successive addition of 0.1 mmol/L H_2O_2 , 0.2 mmol/L Glu, 0.2 mmol/L Fru, 0.2 mmol/L UA, 0.2 mmol/L AA, 0.2 mmol/L OA, 0.2 mmol/L CA and 0.1 mmol/L H_2O_2 at -0.25 V in 10 mL PBS. (D) Amperometric curve of successive addition of milk containing H_2O_2 in 0.1 mol/L PBS.

3.5. Anti-Interference Studies and Real Samples Analysis

The selectivity is also a significant analytical factor for sensors, and several common interfering species were chosen to evaluate the selectivity of the flexible Pt/rGOP electrode. Figure 8C represents the typical amperometric responses upon successive addition of 0.1 mmol/L H_2O_2 , 0.2 mmol/L glucose (Glu), 0.2 mmol/L fructose (Fru), 0.2 mmol/L uric acid (UA), 0.2 mmol/L ascorbic acid (AA), 0.2 mmol/L oxalic acid (OA) and 0.2 mmol/L citric acid (CA) into 0.1 mol/L PBS. The result shows that these potential interfering substances do not exhibit obvious amperometric signals and proves the flexible Pt/rGOP electrode has an excellent selectivity to H_2O_2 .

Food safety has aroused concern with the improvement of the quality of life. Residual hydrogen peroxide is often found in milk, so the sensor can be used to determine H_2O_2 in milk. The amperometric curve of successive addition of H_2O_2 is shown in the Figure 8D. The Pt/rGOP electrode does not exhibit an obvious amperometric response towards pure milk. When the milk contains H_2O_2 , the electrode shows an obvious amperometric response, which is similar in the case of successive addition of H_2O_2 without milk under the same concentration, as shown in Figure 7C. The result indicates that the Pt/rGOP electrode has excellent practical application.

4. Conclusions

In this work, we have developed a facile vacuum filtration method to prepare free-standing GOP, and it can be easily reduced by HI to rGOP. The as-prepared rGOP is made up of multilayer reduced graphene oxide whose thickness could be easily controlled. PtNPs were electrodeposited on rGOP and it thus remarkably increases active surface area and speeds up electron charge-transfer. The amperometric responses of Pt/rGOP towards H_2O_2 are wider from 0.2 $\mu\text{mol/L}$ to 8.5 mmol/L, and the detection ranges are divided into two linear sections: 0.2 $\mu\text{mol/L}$ to 2.0 mmol/L and 2.0 to 8.5 mmol/L. The sensitivity of the sensor is much higher than previous reported ones, and the detection limit of H_2O_2 can be as low as 100 nmol/L ($S/N = 3$). Furthermore, the sensor has long-term stability and nearly retains 92% of original response after being bent 200 times. This flexible sensor is an effective and fascinating tool for quantitative and qualitative monitoring of H_2O_2 in future biomedical and environmental application.

Author Contributions: R.-M.S. prepared the samples and carry out most of experiments; Z.-H.L. and P.-J.W. helped for the electrochemical tests; X.-L.Z. and C.C. helped for the analysis and preparation of manuscript; Z.-G.Z. was in charge of the ideals and gave the support for the whole work.

Acknowledgments: This work was supported by the National Natural Science Foundation of China (Nos. 61471233, 21504051), the Program for Professor of Special Appointment (Eastern Scholar) at SIHL, and the Graduate Program Foundation of Shanghai Polytechnic University (EGD17YJS035).

Conflicts of Interest: The authors declare no conflict of interest.

References

1. Qu, L.; Liu, Y.; He, S.; Chen, J.; Liang, Y.; Li, H. Highly selective and sensitive surface enhanced Raman scattering nanosensors for detection of hydrogen peroxide in living cells. *Biosens. Bioelectron.* **2016**, *77*, 292–298. [[CrossRef](#)] [[PubMed](#)]
2. Droge, W.; Schipper, H.M. Oxidative stress and aberrant signaling in aging and cognitive decline. *Aging Cell* **2007**, *6*, 361–370. [[CrossRef](#)] [[PubMed](#)]
3. Chen, C.; Zhao, X.L.; Li, Z.H.; Zhu, Z.G.; Qian, S.H.; Flewitt, A.J. Current and emerging technology for continuous glucose monitoring. *Sensors* **2017**, *17*, 182. [[CrossRef](#)] [[PubMed](#)]
4. Finkel, T.; Holbrook, N.J. Oxidants: Oxidative stress and the biology of aging. *Nature* **2000**, *408*, 239–247. [[CrossRef](#)] [[PubMed](#)]
5. Schumacker, P.T. Reactive oxygen species in cancer cells: Live by the sword die by the sword. *Cancer Cell* **2006**, *9*, 175–176. [[CrossRef](#)] [[PubMed](#)]
6. Wu, L.; Yin, W.; Tan, X.; Wang, P.; Ding, F.; Zhang, H.; Wang, B.; Zhang, W.; Han, H. Direct reduction of HAuCl_4 for the visual detection of intracellular hydrogen peroxide based on Au-Pt/ SiO_2 nanospheres. *Sens. Actuators B Chem.* **2017**, *248*, 367–373. [[CrossRef](#)]
7. Benvidi, A.; Nafar, M.T.; Jahanbani, S.; Tezerjani, M.D.; Rezaeinasab, M.; Dalirnasab, S. Developing an electrochemical sensor based on a carbon paste electrode modified with nano-composite of reduced graphene oxide and CuFe_2O_4 nanoparticles for determination of hydrogen peroxide. *Mater. Sci. Eng. C* **2017**, *75*, 1435–1447. [[CrossRef](#)] [[PubMed](#)]
8. Tang, B.; Zhang, L.; Xu, K. FIA-near-infrared spectrofluorimetric trace determination of hydrogen peroxide using tricarchlorobocyanine dye and horseradish peroxidase (HRP). *Talanta* **2006**, *68*, 876–882. [[CrossRef](#)] [[PubMed](#)]

9. Brumaghim, J.L.; Li, Y.; Henle, E.; Linn, S. Effects of hydrogen peroxide upon nicotinamide nucleotide metabolism in *Escherichia coli* changes in enzyme levels and nicotinamide nucleotide pools and studies of the oxidation of NADH by Fe (III). *J. Biol. Chem.* **2003**, *278*, 42495–42504. [[CrossRef](#)] [[PubMed](#)]
10. Tahirovic, A.; Copra, A.; Omanovic-Miklicanin, E.; Kalcher, K. A chemiluminescence sensor for the determination of hydrogen peroxide. *Talanta* **2007**, *72*, 1378–1385. [[CrossRef](#)] [[PubMed](#)]
11. Chai, X.; Hou, Q.; Luo, Q.; Zhu, J. Rapid determination of hydrogen peroxide in the wood pulp bleaching streams by a dual-wavelength spectroscopic method. *Anal. Chim. Acta* **2004**, *507*, 281–284. [[CrossRef](#)]
12. Steinberg, S.M. High-performance liquid chromatography method for determination of hydrogen peroxide in aqueous solution and application to stimulated martian soil and related materials. *Environ. Monit. Assess.* **2013**, *185*, 3749–3757. [[CrossRef](#)] [[PubMed](#)]
13. Ge, S.; Liu, W.; Liu, H.; Liu, F.; Yu, J.; Yan, M.; Huang, J. Colorimetric detection of the flux of hydrogen peroxide released from living cells based on the high peroxidase-like catalytic performance of porous PtPd nanorods. *Biosens. Bioelectron.* **2015**, *71*, 456–462. [[CrossRef](#)] [[PubMed](#)]
14. Matoba, T.; Shimokawa, H.; Morikawa, K.; Kubota, H.; Kunihiro, I.; Urakami-Harasawa, L.; Mukai, Y.; Hirakawa, Y.; Akaike, T.; Takeshita, A. Electron spin resonance detection of hydrogen peroxide as an endothelium-derived hyperpolarizing factor in porcine coronary microvessels. *Arterioscler. Thromb. Vasc. Biol.* **2003**, *23*, 1224–1230. [[CrossRef](#)] [[PubMed](#)]
15. Pourbeyram, S. Electrocatalytic determination of H₂O₂ on the electrode modified by LBL assembly of polyoxometalates via zirconium ion glue. *Sens. Actuators B Chem.* **2014**, *192*, 105–110. [[CrossRef](#)]
16. Zhao, X.L.; Li, Z.H.; Chen, C.; Wu, Y.H.; Zhu, Z.G.; Zhao, H.L.; Lan, M.B. A novel biomimetic hydrogen peroxide biosensor based on Pt flowers-decorated Fe₃O₄/graphene nanocomposite. *Electroanalysis* **2017**, *29*, 1518–1523. [[CrossRef](#)]
17. Chen, S.; Yuan, R.; Chai, Y.; Hu, F. Electrochemical sensing of hydrogen peroxide using metal nanoparticles: A review. *Microchim. Acta* **2013**, *180*, 15–32. [[CrossRef](#)]
18. Chen, X.; Wu, G.; Cai, Z.; Oyama, M.; Chen, X. Advances in enzyme-free electrochemical sensors for hydrogen peroxide, glucose, and uric acid. *Microchim. Acta* **2014**, *181*, 689–705. [[CrossRef](#)]
19. Zhu, Z.G.; Garcia-Gancedo, L.; Chen, C.; Zhu, X.R.; Xie, H.Q.; Flewitt, A.J.; Milne, W.I. Enzyme-free glucose biosensor based on low density CNT forest grown directly on a Si/SiO₂ substrate. *Sens. Actuators B Chem.* **2013**, *178*, 586–592. [[CrossRef](#)]
20. Hsu, S.Y.; Lee, C.L. Sonoelectrochemical exfoliation of highly oriented pyrolytic graphite for preparing defective few-layered graphene with promising activity for non-enzymatic H₂O₂ sensors. *Microchim. Acta* **2017**, *184*, 2489–2496. [[CrossRef](#)]
21. Wen, Y.; Wen, W.; Zhang, X.; Wang, S. Highly sensitive amperometric biosensor based on electrochemical-reduced graphene oxide chitosan/hemoglobin nanocomposite for nitromethane determination. *Biosens. Bioelectron.* **2016**, *79*, 894. [[CrossRef](#)] [[PubMed](#)]
22. Novoselov, K.S.; Geim, A.K.; Morozov, S.V.; Jiang, D.; Zhang, Y.; Dubonos, S.V.; Grigorieva, I.V.; Firsov, A.A. Electric field effect in atomically thin carbon films. *Science* **2004**, *306*, 666–669. [[CrossRef](#)] [[PubMed](#)]
23. Zheng, Y.; Wang, A.; Lin, H.; Fu, L.; Cai, W. A sensitive electrochemical sensor for direct phoxim detection based on electrodeposited reduced graphene oxide-gold nanocomposite. *RSC Adv.* **2015**, *5*, 15425–15430. [[CrossRef](#)]
24. Yaldagard, M.; Seghatoleslami, N.; Jahanshahi, M. Preparation of Pt-Co nanoparticles by galvanostatic pulse electrochemical codeposition on in situ electrochemical reduced graphene nanoplates based carbon paper electrode for oxygen reduction reaction in proton exchange membrane fuel cell. *Appl. Surf. Sci.* **2014**, *315*, 222–234. [[CrossRef](#)]
25. Zhu, Z.G.; Garcia-Gancedo, L.; Flewitt, A.J.; Xie, H.Q.; Moussy, F.; Milne, W.I. A critical review of glucose biosensors based on carbon nanomaterials: Carbon nanotubes and graphene. *Sensors* **2012**, *12*, 5996–6022. [[CrossRef](#)] [[PubMed](#)]
26. Obraztsov, A.N. Chemical vapour deposition: Making graphene on a large scale. *Nat. Nanotechnol.* **2009**, *4*, 212–213. [[CrossRef](#)] [[PubMed](#)]
27. Su, C.; Lu, A.; Xu, Y.; Chen, F.; Khlobystov, A.N.; Li, L. High-quality thin graphene films from fast electrochemical exfoliation. *ACS Nano* **2011**, *5*, 2332–2339. [[CrossRef](#)] [[PubMed](#)]

28. Berger, C.; Song, Z.; Li, X.; Wu, X.; Brown, N.; Naud, C.; Mayou, D.; Li, T.; Hass, J.; Marchenkov, A.; et al. Electronic confinement and coherence in patterned epitaxial graphene. *Science* **2006**, *312*, 1191–1196. [[CrossRef](#)] [[PubMed](#)]
29. Yang, J.; Gunasekaran, S. Electrochemically reduced graphene oxide sheets for use in high performance supercapacitors. *Carbon* **2013**, *51*, 36–44. [[CrossRef](#)]
30. Lei, Z.; Lu, L.; Zhao, X. The electrocapacitive properties of graphene oxide reduced urea. *Energy Environ. Sci.* **2012**, *5*, 6391–6399. [[CrossRef](#)]
31. Chen, Y.; Zhang, X.; Zhang, D.; Yu, P.; Ma, Y. High performance supercapacitors based on reduced graphene oxide in aqueous and ionic liquid electrolytes. *Carbon* **2011**, *49*, 573–580. [[CrossRef](#)]
32. Choi, E.Y.; Han, T.H.; Hong, J.; Kim, J.E.; Lee, S.H.; Kim, H.W.; Kim, S.O. Noncovalent functionalization of graphene with end-functional polymers. *J. Mater. Chem.* **2010**, *20*, 1907–1912. [[CrossRef](#)]
33. Zhu, Y.; Stoller, M.D.; Cai, W.; Velamakanni, A.; Piner, R.D.; Chen, D.; Ruoff, R.S. Exfoliation of graphene oxide in propylene carbonate and thermal reduction of the resulting graphene oxide platelets. *ACS Nano* **2010**, *4*, 1227–1233. [[CrossRef](#)] [[PubMed](#)]
34. Yang, J.; Deng, S.; Lei, J.; Ju, H.; Gunasekaran, S. Electrochemical synthesis of reduced graphene sheet-AuPd alloy nanoparticle composites for enzymatic biosensing. *Biosens. Bioelectron.* **2011**, *29*, 159–166. [[CrossRef](#)] [[PubMed](#)]
35. Guo, H.; Wang, X.; Qian, Q.; Wang, F.; Xia, X. A green approach to the synthesis of graphene nanosheets. *ACS Nano* **2009**, *3*, 2653–2659. [[CrossRef](#)] [[PubMed](#)]
36. Peng, X.; Liu, X.; Diamond, D.; Lau, K.T. Synthesis of electrochemically-reduced graphene oxide film with controllable size and thickness and its use in supercapacitor. *Carbon* **2011**, *49*, 3488–3496. [[CrossRef](#)]
37. Zhu, Y.; Murali, S.; Stoller, M.D.; Ganesh, K.J.; Cai, W.; Ferreira, P.J.; Pirkle, A.; Wallace, R.M.; Cychosz, K.A.; Thommes, M.; et al. Carbon-Based supercapacitors produced by activation of graphene. *Science* **2011**, *332*, 1537–1541. [[CrossRef](#)] [[PubMed](#)]
38. Zhu, Y.; Murali, S.; Stoller, M.D.; Velamakanni, A.; Piner, R.D.; Ruoff, R.S. Microwave assisted exfoliation and reduction of graphite oxide for ultracapacitors. *Carbon* **2010**, *48*, 2106–2122. [[CrossRef](#)]
39. Dikin, D.A.; Stankovich, S.; Zimney, E.J.; Piner, R.D.; Dommett, G.H.B.; Evmenenko, G.; Nguyen, S.T.; Ruoff, R.S. Preparation and characterization of graphene oxide paper. *Nature* **2007**, *448*, 457–460. [[CrossRef](#)] [[PubMed](#)]
40. Chen, H.; Muller, M.B.; Gilmore, K.J.; Wallace, G.G.; Li, D. Mechanically strong, electrically conductive, and biocompatible graphene paper. *Adv. Mater.* **2008**, *20*, 3557–3561. [[CrossRef](#)]
41. Li, D.; Muller, M.B.; Gilje, S.; Kaner, R.B.; Wallace, G.G. Processable aqueous dispersions of graphene nanosheets. *Nat. Nanotechnol.* **2008**, *3*, 101–105. [[CrossRef](#)] [[PubMed](#)]
42. Sun, S.; Yang, D.; Villers, D.; Zhang, G.; Sacher, E.; Dodelet, J.P. Template- and surfactant-free room temperature synthesis of self-assembled 3D Pt nanoflowers from single-crystal nanowires. *Adv. Mater.* **2008**, *20*, 571–574. [[CrossRef](#)]
43. Pang, Y.; Zhang, Y.; Li, W.; Ding, H.; Shen, X. Synergetic accumulation and simultaneous determination of naphthol isomers on electrochemically reduced graphene oxide modified electrode. *J. Electroanal. Chem.* **2016**, *769*, 89–96. [[CrossRef](#)]
44. Zhu, Z.G.; Garcia-Gancedo, L.; Flewitt, A.J.; Moussy, F.; Li, Y.; Milne, W.I. Design of carbon nanotube fiber microelectrode for glucose biosensing. *J. Chem. Technol. Biotechnol.* **2011**, *87*, 256–262. [[CrossRef](#)]
45. Ghaderi, S.; Mehrgardi, M.A. Prussian blue-modified nanoporous gold film electrode for amperometric determination of hydrogen peroxide. *Bioelectrochemistry* **2014**, *98*, 64–69. [[CrossRef](#)] [[PubMed](#)]
46. Zhang, M.; Halder, A.; Hou, C.; Ulstrup, J.; Chi, Q. Free-standing and flexible graphene papers as disposable non-enzymatic electrochemical sensors. *Bioelectrochemistry* **2016**, *109*, 87–107. [[CrossRef](#)] [[PubMed](#)]
47. Xiao, F.; Song, J.; Gao, H.; Zan, X.; Xu, R.; Duan, H. Coating graphene paper with 2D-assembly of electrocatalytic nanoparticles: A modular approach toward high performance flexible electrodes. *ACS Nano* **2012**, *6*, 100–110. [[CrossRef](#)] [[PubMed](#)]
48. Liang, B.; Fang, L.; Hu, Y.; Yang, G.; Zhu, Q.; Ye, X.S. Fabrication and application of flexible graphene silk composite film electrodes decorated with spiky Pt nanospheres. *Nanoscale* **2014**, *6*, 4264–4274. [[CrossRef](#)] [[PubMed](#)]
49. Xiao, F.; Li, Y.; Zan, X.; Liao, K.; Xu, R.; Duan, H. Growth of metal-metal oxide nanostructures on freestanding graphene paper for flexible biosensors. *Adv. Funct. Mater.* **2012**, *22*, 2487–2494. [[CrossRef](#)]

50. Zhang, Q.; Qiao, Y.; Zhang, L.; Wu, S.; Zhou, H.; Xu, J.; Song, X. Direct electrochemistry and electrocatalysis of horseradish peroxidase immobilized on water soluble sulfonated graphene film via self-assembly. *Electroanalysis* **2011**, *23*, 900–906. [[CrossRef](#)]
51. Zhong, L.; Gan, S.; Fu, X.; Li, F.; Han, D.; Guo, L.; Niu, L. Electrochemically controlled growth of silver nanocrystals on graphene thin film and applications for efficient nonenzymatic H₂O₂ biosensor. *Electrochim. Acta* **2013**, *89*, 222–228. [[CrossRef](#)]
52. Xi, Q.; Chen, X.; Evans, D.G.; Yang, W. Gold nanoparticle-embedded porous graphene thin films fabricated via layer-by-layer self-assembly and subsequent thermal annealing for electrochemical sensing. *Langmuir* **2012**, *28*, 9885–9892. [[CrossRef](#)] [[PubMed](#)]



© 2018 by the authors. Licensee MDPI, Basel, Switzerland. This article is an open access article distributed under the terms and conditions of the Creative Commons Attribution (CC BY) license (<http://creativecommons.org/licenses/by/4.0/>).